Thermochimica Acta 716 (2022) 179318

Contents lists available at ScienceDirect

Thermochimica Acta

journal homepage: www.elsevier.com/locate/tca

# High-pressure crystallization of iPP nanocomposites with montmorillonite and carbon nanotubes

Przemyslaw Sowinski [a,*], Sivanjineyulu Veluri [a], Ewa Piorkowska [a,*], Konrad Kwiecinski [a], Severine A.E. Boyer [b], Jean-Marc Haudin [b]

[a] Centre of Molecular and Macromolecular Studies, Polish Academy of Sciences, Sienkiewicza 112, Lodz 90 363, Poland
[b] Centre for Material Forming, MINES ParisTech, PSL-Research University, UMR CNRS 7635, 1 Rue Claude Daunesse, Sophia Antipolis 06904, France

ARTICLE INFO

*Keywords:*
Crystallization under high pressure
γ-form
Nanocomposites
Thermal properties
Polymer composites

ABSTRACT

High pressure facilitates crystallization of isotactic polypropylene (iPP) in the orthorhombic γ-form, differing in structure and properties from the α-form, in which iPP crystallizes under common processing conditions. In the study, the effect of high pressure on crystallization of iPP nanocomposites was examined. The iPP nanocomposites with 1-5 wt.% of well dispersed either o-MMT (PP/MT) or MWCNT (PP/CN) were prepared by mixing molten iPP with the nanofillers. The nanocomposites and neat iPP were crystallized during cooling under pressures up to 300 MPa. Regardless of crystallization pressure, the crystallization temperatures were similar whereas the sizes of the polycrystalline aggregates were only slightly smaller in PP/MT compared to those of neat iPP. On the contrary, the presence of MWCNT elevated the crystallization temperature of PP/CN by 8-13 K compared to that of neat iPP, and strongly decreased the grain size. This evidenced the nucleating activity of MWCNT during high-pressure crystallization of iPP in the γ-form. The higher crystallization temperature allowed a larger portion of the polymer to crystallize in the γ-domain before the α-domain was reached. As a result, PP/CN, especially crystallized under 50-100 MPa, contained more γ-form than neat iPP and PP/MT.

## 1. Introduction

One of the most important commodity thermoplastics is isotactic polypropylene (iPP). iPP is a stereo-regular polymer that can crystallize in various crystallographic forms such as monoclinic α, trigonal β, orthorhombic γ, and in the so-called "smectic mesophase", distinguished by the arrangement of the chains. The monoclinic α-form is the most common and prevails in the iPP processed under atmospheric pressure. By contrast, the trigonal β-phase can be observed at specific conditions of crystallization, including zone solidification [1] or the use of special nucleating agents [2,3]. The formation of smectic mesophase was observed at very high undercoolings [4]. The γ-phase was found in low molar mass iPP [5–7], in propylene copolymers with a small content of 1-olefine co-units [8–11], and also in iPP with stereo- or regio-defects [12–14]. De Rosa et al. [13] found that the content of γ-form in iPP depended on the concentration and distribution of defects. Moreover, the formation of the γ-phase in highly stereoregular iPP homopolymer was facilitated under high pressure [15,16]. It is worth mentioning that the trigonal modification, termed δ, was found in the copolymers of propylene with more than 10% of hexene or pentene comonomers, due to their longer side chains [17,18]. Moreover, in stereo-defective iPP the orthorhombic ε-form was also discovered, which was nucleated on the α-form lamellae [19].

Among these crystallographic forms, the γ-form has received considerable attention because of its unique structure without the parallel arrangement of chain axes, unlike in other known polymer crystals. The γ-lamellae are built of successive bi-layers of parallel chains, in which the chain axes are inclined by ca.80° to those in the neighboring bi-layers [20–22]. The γ-iPP crystallized under high pressure can exhibit mechanical properties different than those of α-iPP due to the unique structure of γ-crystals, and in consequence, the mechanism of plastic deformation in γ-iPP differs from that in α-iPP [23–25]. The Young modulus and yield stress of γ-iPP deformed in compression exceeded by 75-80% those of α-iPP tested in the same way [23]. The high yield stress of γ-iPP was also reported in [24]. It is worth mentioning that not only a high pressure is necessary to crystallize iPP in the γ-form, but also a high temperature, especially because the phase transition temperatures of polymers increase with increasing pressure.

* Corresponding authors.
*E-mail addresses:* przem_so@cbmm.lodz.pl (P. Sowinski), epiorkow@cbmm.lodz.pl (E. Piorkowska).

https://doi.org/10.1016/j.tca.2022.179318
Received 6 April 2022; Received in revised form 12 August 2022; Accepted 13 August 2022
Available online 14 August 2022

Mezghani and Phillips [26] formulated a temperature-pressure phase diagram for the α-form and γ-form of iPP and also determined the dependence of equilibrium melting temperature ($T_m^0$) of both forms on crystallization pressure. As the pressure dependence of transition temperature between the α- and γ-domains is not so strong as that of $T_m^0$, the γ-domain broadens with increasing pressure.

Moreover, the high-pressure crystallization of iPP in the γ-form can be enhanced by the use of appropriate nucleating agents. We have previously demonstrated that the commercial nucleants, nucleating the α-form under atmospheric pressure, were efficient in nucleating the crystallization of iPP in the γ-form under high pressure [27–30]. The activity of those nucleants shifted up the crystallization temperature range during cooling and strongly decreased the size of polycrystalline aggregates of iPP. The same was observed in iPP nanocomposites with fibrillated poly(tetrafluoroethylene) [31], which is known to effectively nucleate the α-form of iPP under atmospheric pressure [31–33] and the γ-form under elevated pressure [27–29,31].

We have demonstrated previously that the γ-lamellae were formed predominantly through epitaxy on the α-lamellae, which nucleated first on the nucleant particles and served as seeds for the γ-phase [29]. It is also worth mentioning that during cooling under elevated pressure, especially below 200 MPa, the crystallization of iPP may not be accomplished in the γ-domain and therefore continues in the α-domain, which leads to the formation of a considerable amount of the α-phase. Under such conditions, the activity of nucleants enlarged the γ-content because of the elevation of crystallization temperature and the shortening of crystallization [27–31].

Filling is a well-known method of modification of polymer properties. It has been recognized that the addition of nano-sized particles, for instance, silica, titanium dioxide ($TiO_2$), graphene oxide (GO), carbon nanotubes (CNT) and organo-modified montmorillonite (o-MMT) to semicrystalline polymers can profoundly change their performance [34–41]. CNT and o-MMT are long known as efficient reinforcements in iPP based nanocomposites [42–44], although the effect is not only related to the nanofiller intrinsic properties but also to their surface modification, dispersion, and orientation. Well dispersed CNT and o-MMT particles can affect mechanical, thermal and barrier properties of nanocomposites, among others. Moreover, the low content of CNT is sufficient to impart electrical conductivity to polymeric materials [42,45,46] making them suitable for applications such as electromagnetic shielding, anti-electrostatic materials, electrodes, etc. Nanofillers frequently influence crystallization of polymer matrix through nucleating activity, affecting the growth of crystals or inducing crystallization in a different crystallographic form [47]. Both, CNT and o-MMT were found to affect crystallization of polymers, including iPP. The ability of both single-wall and multi-wall CNT to nucleate iPP crystallization in the α-form was observed during both isothermal and nonisothermal crystallization, leading to a decrease of spherulite size, an acceleration of the crystallization, and an increase of crystallization temperature during cooling [42,48–51]. The effects depended on CNT concentration and saturated with its increase [48,51,52] due to agglomeration [52]. However, it was also reported that CNT can hinder the growth of iPP crystals [48]. Lu et al. [53] observed the formation of highly oriented transcrystalline layers around nucleating CNT, with the crystallographic c-axes oriented perpendicular to the nanotube long axes. Grady et al. [54] found that CNT promoted the growth of the β-form of iPP at the expense of the α-form. In turn, Zhang et al. [55] found the γ-form crystals in transcrystalline zones nucleated on CNT. Lin et al. [56] studied the effect of CNT on shear-induced isothermal crystallization of iPP under moderate pressure, up to 150 MPa. The addition of the nanotubes promoted the formation of oriented crystals. However, under 50 and 100 MPa, the presence of CNT decreased the content of the γ-form in the sheared nanocomposite compared to neat iPP. It is worth mentioning, that Wang et al. [57] observed shear-induced acceleration of isothermal crystallization of iPP with CNT, although the effect decreased and finally vanished with a decrease of crystallization temperature.

The properties of polymer nanocomposites with o-MMT depend to a great extent on the level of exfoliation of the clay platelets. To achieve o-MMT exfoliation in iPP, maleic anhydride grafted polypropylene (PP-g-MA) was frequently used as a compatibilizer or even as a matrix. The effect of o-MMT on both isothermal and nonisothermal crystallization of iPP was extensively studied [47]. A decrease of spherulite size, an acceleration of crystallization and an increase of the nonisothermal crystallization peak temperature of the matrix due to the presence of o-MMT was reported [55,58–64]. Noteworthy, in the investigated systems a significant amount of intercalated clay tactoids was present [58,59,63,64]. However, when fine clay dispersion was achieved the nucleating effect of the clay was limited [63,64]. It was also reported that the dispersed clay platelets can hinder the growth of iPP crystals [64]. Moreover, the γ-phase was detected in PP-g-MA nanocomposites with o-MMT, and its content increased with increasing clay content [62]. Studies of isothermal crystallization of iPP nanocomposites with o-MMT under elevated pressure [65,66] demonstrated that the clay promoted the formation of the γ-phase even under low pressure. It is worth mentioning that the enhancement of the effect of shear flow on crystallization of iPP due to the presence of o-MMT was also observed [67,68].

During injection molding, polymer materials are subjected to high pressure and usually crystallize nonisothermally during processing. Our current study focuses on the nonisothermal crystallization of iPP based nanocomposites with o-MMT and multiwall CNT (MWCNT) under high pressure, up to 300 MPa. Nanocomposites with 1-5 wt.% of the nanofillers were prepared by melt compounding and their structure was examined by transmission electron microscopy (TEM) and X-ray diffraction (XRD), whereas their thermal properties were characterized by thermogravimetry (TGA) and differential scanning calorimetry (DSC). The influence of the nanofillers on the nonisothermal crystallization temperature of iPP under various pressures was determined. After the crystallization, the nanocomposites were examined by wide angle X-ray diffraction (WAXD), polarized light microscopy (PLM), and DSC. It was found that the effect of o-MMT on the high-pressure crystallization of iPP was minor. On the contrary, the activity of MWCNT in the nucleation of the high-pressure crystallization of iPP in the γ-form elevated the crystallization temperature and dramatically reduced the sizes of polycrystalline aggregates. It also increased the γ-content, especially under the pressure of 50 and100 MPa. Under 200 and 300 MPa the materials crystallized in nearly pure or pure γ-form.

## 2. Experimental

### 2.1. Materials

Isotactic polypropylene (PP) Adstif HA740N (melt flow rate of 12 g/10 min at 230°C/2.16 kg, density of 0.9 g/cm$^3$) was supplied by Basell Orlen Polyolefins (Poland). Anox 20 and Ultranox 626 were purchased from Addivant (USA). Cloisite C15A, dimethyl di(hydrogenated tallow) quaternary ammonium modified o-MMT, was purchased from Southern Clay Products (USA). According to the producer $d_{001}$ spacing of o-MMT was 3.15 nm and its particle size was below 13 μm [69]. Maleic anhydride grafted polypropylene (PP-g-MA), Polybond 3150 from Chemtura Corporation (USA), with 0.5 wt. % of MA groups, density of 0.91 g/cm$^3$ and MFR of 50 g/10 min (230°C/2.16 kg), was used to compatibilize o-MMT with PP. Plasticyl PP2001, masterbatch of iPP loaded with 20 wt.% of MWCNT NC7000, with density of 0.872 g/cm$^3$, was purchased from Nanocyl (USA). According to the supplier, an average diameter of MWCNT was 9.5 nm, average length 1.5 μm, carbon purity 90%, and surface area 250-300 m$^2$/g [70].

### 2.2. Nanocomposite preparation

To prepare PP nanocomposites with o-MMT, first, a masterbatch of o-

MMT with PP-g-MA compatibilizer, with a weight ratio of 1:2, was obtained by mixing the components in BTSK 20/40D twin screw co-rotating intermeshing extruder at 20 rpm, in a temperature range of 185-195°C. PP nanocomposites with o-MMT (PP/MT) and MWCNT (PP/CN) were prepared by blending the components in a Brabender batch mixer at 195°C. At first, PP was mixed with 0.2 wt.% of Anox 20, 0.2 wt.% of Ultranox 626 and 0.2 wt.% of calcium stearate at 195°C for 6 min at 60 rpm. Next, appropriate amounts of the masterbatch of PP-g-MA with o-MMT or Plasticyl PP2001 masterbatch were added, to obtain nanofiller content of 1, 3 and 5 wt.%. Then, the rotation speed was increased, within 4 min, every minute by 10 rpm, and the mixing was continued for the next 10 min at 100 rpm. As a reference, the neat PP was also processed in the same way. The component content in the nanocomposites is listed in Table 1 together with sample codes.

### 2.3. Crystallization under high pressure

The specimens in the form of disks with diameters of 9.5 mm (approx. 200 mg) were placed in a custom-built cell made of ultra high-strength steel, with a channel and piston, as described in detail elsewhere [27–31,71]. To pressurize, the specimens in the molten state were compressed in the cell using Instron tensile testing machine (Instron Corp., High Wycombe, UK) at a crosshead speed of 2 mm/min via a fixture that stabilized the load exactly along the cell axis. The temperature and hydrostatic pressure in the cell were controlled with an accuracy of 1 K and 0.5 MPa, respectively. The pressure and temperature protocol is schematically presented in Fig. 1.

At first the pressure was increased to 1.3 MPa to provide good thermal contacts in the cell. Then, the cell was heated 230°C and the temperature was held at this level for 3 min to destroy the thermal history of specimens. Next, the pressure was increased, during approx. 2 min, to the selected value, ranging from 50 to 300 MPa. Then, the cell was cooled down, still under the elevated pressure, to about 40°C, and the pressure was released. The crystallization of all materials under 1.3 MPa pressure was also conducted. Structure and thermal properties of the crystallized specimens were examined *ex-situ* by WAXD, PLM and DSC. The rate of cooling of the cell was reproducible, although not controlled, and it was nearly constant, approx. 8°C/min, in the temperature range of crystallization of PP based materials.

The measurement of the time dependence of crosshead displacement during cooling of the cell under elevated pressure allowed to determine the displacement rate, which exhibited a peak. The peak corresponded to the volume change rate of specimen related to the specimen crystallization rate. Simultaneous measurement of the temperature allowed to determine the temperature of peak rate, which was taken as the crystallization temperature ($T_c$), as it was described previously [27]. Exemplary plots of the crosshead displacement rate are shown in Fig. S1 in Supplementary Information (SI).

### 2.4. Characterization

To study the dispersion of the nanofillers in the nanocomposites, TEM was carried out using modernized TESLA BS 500 (The Czech Republic) with tungsten filament at an accelerating voltage of 90 kV. Ultra-thin sections (ca. 60 nm thick) for TEM analysis were microtomed using an ultramicrotome PC PowerTome from Boeckerel (USA) equipped with a diamond knife.

**Table 1**
Sample codes and component content in nanocomposites.

| Sample code | Component content (wt.%) | | | |
|---|---|---|---|---|
| | PP | PP-g-MA | o-MMT | CNT |
| PP | 100 | — | — | — |
| PP/MT1 | 97 | 2 | 1 | — |
| PP/MT3 | 91 | 6 | 3 | — |
| PP/MT5 | 85 | 10 | 5 | — |
| PP/CN1 | 99 | — | — | 1 |
| PP/CN3 | 97 | — | — | 3 |
| PP/CN5 | 95 | — | — | 5 |

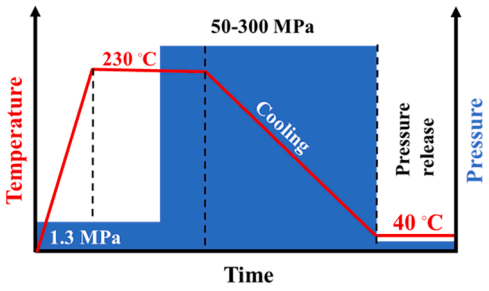


**Fig. 1.** Scheme of pressure and temperature protocol.

To examine the exfoliation of o-MMT in PP/MT nanocomposites, XRD in the transmission mode, in a 2θ range of 1-9°, was performed, as previously described [68]. To eliminate the effect of possible orientation of o-MMT in the studied specimens, PP/MT nanocomposites were cryo-ground and the powdered materials were used to fill a cell placed in an X-ray diffractometer [67,68]. The o-MMT powder was also examined for comparison.

The structure of the crystallized materials was studied by WAXD in the reflection mode using Panalytical Xpert' PRO diffraction system from Malvern Panalytical Ltd. (UK), operating at 40 kV and 30 mA, with CuKα radiation (0.154056 nm). The diffractograms were collected in a 2θ range of 10–70° and then deconvoluted using WAXSFIT program [72], as previously described [27–31]. The equation proposed by Turner-Jones et al. [73] was used to determine the content of the α- and γ-phases in the crystalline phase ($K_\alpha$ and $K_\gamma$) based on the integral intensities, I, of appropriate peaks:

$$K_\gamma = I(117)_\gamma \Big/ \left[\left(I(117)_\gamma + I(130)_\alpha\right]\right. \quad (1a)$$

$$K_\alpha = 1 - K_\gamma \quad (1b)$$

Based on the diffractograms, also a crystallinity degree ($X_c$) was calculated, taking into account the amorphous halos also being determined by the deconvolution.

The semicrystalline morphology of nanocomposites was examined with PLM. Approx. 10 μm thick sections of the materials were microtomed and examined by means of a PZO microscope (Poland) and a video camera.

To study their thermal stability, 10-12 mg specimens were heated at 20 K/min up to 750°C in air and in nitrogen atmosphere in TGA5500 from TA Instruments (USA). In turn, the phase transitions under atmospheric pressure ($P_{atm}$) of 6-8 mg specimens were studied using DSC 2920 from TA Instruments (USA). Their crystallization was studied on cooling at 10 K/min and at 8 K/min, after holding at 230°C for 3 min to destroy thermal history. Melting of the specimens crystallized under various pressures was studied on heating to 230°C at two different heating rates, 10 and 30 K/min.

## 3. Results and discussion

TGA analysis evidenced the good thermal stability of the nanocomposites. Temperatures of 5 wt.% weight loss ($T_{5\%}$) and temperatures of peaks of weight loss derivative with respect to temperature ($T_D$) of the tested materials are collected in Table S1 in SI. $T_{5\%}$ values of the materials in air ranged from 290 to 308°C. The nanocomposites with 3 and 5 wt.% of nanofillers exhibited the highest values of $T_{5\%}$, 299-308°C. Moreover, $T_D$ of the nanocomposites in air, from 385°C to 441°C, markedly exceeded that of neat PP, 355°C. The improvement of thermal stability due to the presence of MWCNT and exfoliated o-MMT was already observed and discussed by others [42,74].

X-ray diffractograms of o-MMT and PP/MT are shown in Fig. S2. A broad peak with a maximum at 2θ of 2.9° on the diffractogram of o-MMT reflected the periodic structure of clay tactoids. Only traces of o-MMT peaks were discernible on the curves of PP/MT, due to the exfoliation of the clay particles. Moreover, they shifted to lower 2θ angles due to the intercalation of remaining o-MMT tactoids with polymer chains. TEM micrographs in Fig. S3 corroborated the dispersion and exfoliation of the clay particles, as well as good dispersion of MWCNT. However, the dispersion of MWCNT worsened with their increasing content resulting in small submicron clusters observed in PP/CN5 by TEM, as shown in Fig. S3.

The influence of the nanofillers on the nonisothermal crystallization of PP under $P_{atm}$ was studied by means of DSC. Fig. 2 shows exemplary cooling thermograms of the materials and PLM micrographs of thin sections of the crystallized specimens. The peak rate of neat PP crystallization was at temperature ($T_c$) of 122°C. PP/MT crystallized in the same temperature range as neat PP, with $T_c$ of 123°C. On the contrary, PP/CN crystallized in the higher temperature range, and their $T_c$s increased, from 126°C for PP/CN1 to 131°C for PP/CN3 and PP/CN5, due to the nucleation activity of MWCNT. Exemplary heating thermograms of the materials presented in Fig. S4, exhibited melting endotherms with single peaks at temperatures ($T_m$) of 166-168°C, and melting enthalpy ($\Delta H_m$) around 100 J/g. The nucleation activity of MWCNT was confirmed by PLM examination, as shown in Fig. 2. Spherulite sizes were similar in PP and PP/MT. On the contrary, fine grain structure was observed in PP/CN due to the intense primary nucleation in these materials.

$T_c$ values of PP/MT and PP/CN during crystallization under various pressures are plotted in Fig. 3. The precise determination of $T_c$ under 1.3 MPa was impossible, thus $T_c$ values measured during cooling of the materials in DSC at 8 K/min are plotted instead. With increasing pressure, $T_c$ of all PP based materials increased, as it was reported by us previously [27,30,31]. It is known that the phase transition temperatures of polymers increase with increasing pressure. Others found that under 200 MPa $T_m^0$ of the γ-form increased to 241°C [26] or to 232°C [32]. By linear extrapolation of the results shown in [26] and [75] the increase of $T_m^0$ by 27 or 19 K, respectively, can be predicted with increasing pressure from 200 to 300 MPa. $T_c$ of neat PP increased from 123°C under $P_{atm}$ to 179°C under 300 MPa. Regardless of the pressure and o-MMT content, $T_c$s of PP/MT were similar to that of neat PP. As it is seen in Fig. 3 the pressure dependencies of $T_c$ of PP and PP/MT overlap. $T_c$ of PP/MT increased from 123-124°C under $P_{atm}$ to 178-180°C under 300 MPa.

Nearly the same $T_c$ values of PP and PP/MT were suggestive of the absence of significant nucleation activity of o-MMT in the nanocomposites. On the contrary, $T_c$s of PP/CN exceeded that of neat PP in the entire pressure range studied and depended on the MWCNT content. $T_c$ of PP/CN1 was higher than that of neat PP by 3-5 K and increased from 127°C under $P_{atm}$ to 184°C under 300 MPa. PP/CN3 and PP/CN5 crystallized at even higher temperature. Their $T_c$s were similar but higher than $T_c$ of neat PP by 7-13 K, increasing from 130-132°C to 190-192°C under 300 MPa. These results indicated that MWCNT nucleated crystallization of PP not only under $P_{atm}$ but also under elevated pressure. This was confirmed by the decrease of polycrystalline aggregate sizes, as seen in PLM micrographs collected in Fig. 4.

The sizes of polycrystalline aggregates in PP/MT were only slightly smaller than in neat PP regardless of the pressure and o-MMT content. On the contrary, fine grain structure was found in PP/CN, especially PP/CN3 and PP/CN5, crystallized in the entire pressure range studied, up to 300 MPa, evidencing the intense nucleation.

WAXD diffractograms of neat PP, PP/MT5, and PP/CN5 crystallized under various pressures are shown in Fig. 5. The diffractograms recorded for the nanocomposites with 1 wt.% and 3 wt.% filler content are not shown because they were very similar to those of PP/MT5 and PP/CN5. As could be expected, the materials crystallized under 1.3 MPa contained predominantly the α-form.

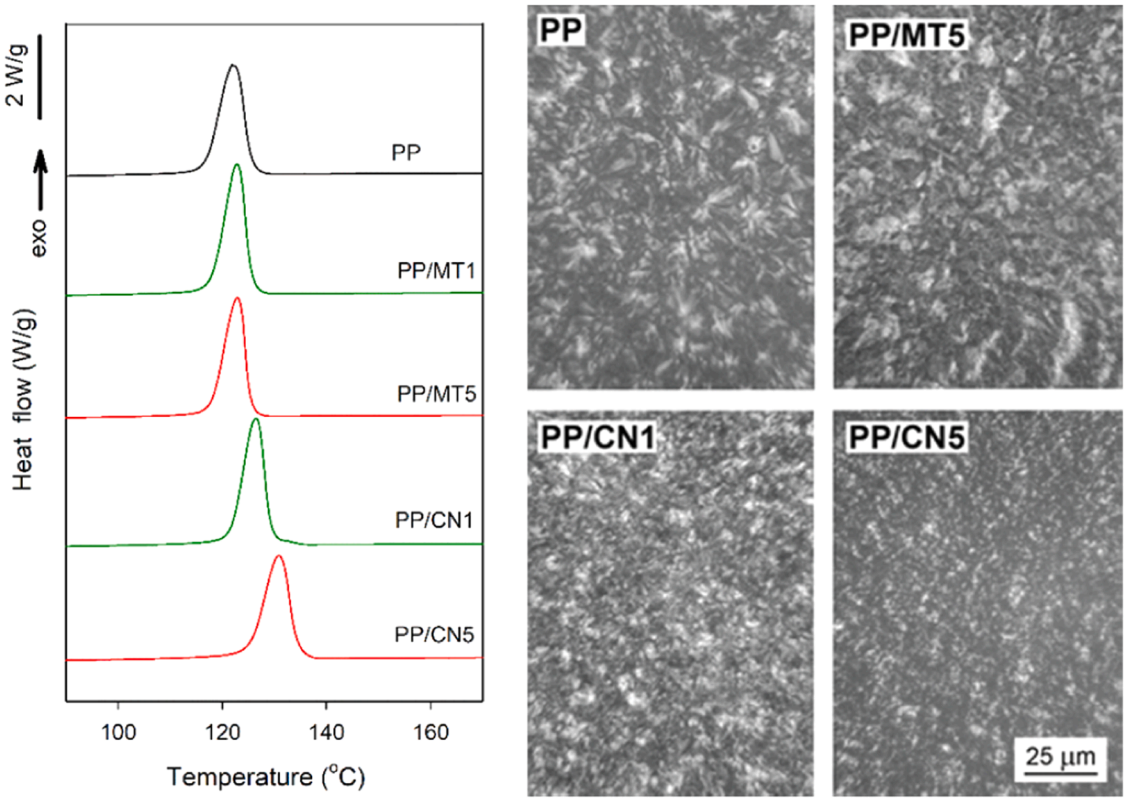


**Fig. 2.** DSC thermograms of neat PP and nanocomposites PP/MT1, PP/MT5, PP/CN1, PP/CN5 during cooling at 10 K/min (left), and PLM micrographs of thin sections of PP and nanocomposites PP/MT5, PP/CN1, PP/CN5 crystallized during cooling (right).

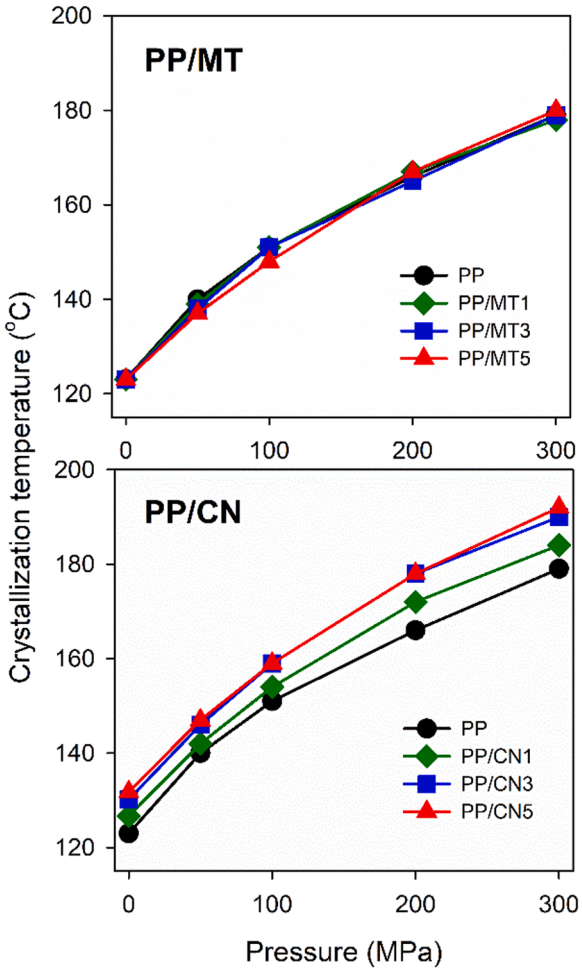


**Fig. 3.** Crystallization temperatures, $T_c$, of neat PP, PP/MT and PP/CN nanocomposites nonisothermally crystallized during cooling under various pressures.

However, weak $(117)_\gamma$ peaks evidenced that in each case the α-form was accompanied by small amount of the γ-form. With increasing pressure, $(117)_\gamma$ peak enlarged, which was accompanied by the decrease of $(130)_\alpha$ peak, indicating the increasing γ-content in the crystalline phase. In the diffractograms of PP/CN $(117)_\gamma$ peak was larger while $(130)_\alpha$ peak was smaller than in the diffractograms of PP and PP/MT, evidencing the higher content of the γ-phase. The absence of $(130)_\alpha$ peak in the diffractograms of the materials crystallized under 300 MPa indicated that the PP matrix crystallized solely in the γ-modification. The phase content, $K_\alpha$ and $K_\gamma$, and also the crystallinity, $X_c$, of all materials studied are plotted in Figs. 6, S4 and listed in Table S2. The increase of pressure resulted in increase of the γ-content in the crystalline phase of all the materials. Under 100 MPa the γ-phase became predominant. Under 200 and 300 MPa the polymer matrix crystallized in nearly pure or pure γ-form.

The γ-content in all PP/MT was similar to that in neat PP. In PP/CN the γ-content was higher than in PP and PP/MT by 2-20%, especially at 50 and 100 MPa, with a tendency to increase with increasing MWCNT content. At 200 MPa $K_\gamma$ of PP/CN reached 1.0 whereas it was slightly smaller in the other materials. During cooling under elevated pressure the crystallization began in the γ-domain. If it was not completed in the γ-domain, it continued in the lower temperature range, in the α-form. An increase of pressure results in broadening of the temperature range of γ-domain, hence in the increase of the γ-content [26]. However, it should be noted that $X_c$ depended strongly neither on the pressure nor on the filler type or content. The larger γ-content in PP/CN resulted from the nucleating activity of MWCNT, reflected in the increase of $T_c$ and the formation of fine-grain structure. The crystallization in the higher temperature range from more numerous nucleation sites resulted in a larger portion of the polymer solidified in the γ-domain, which left less polymer melt to crystallize in the α-form in the lower temperature range. At 50 and 100 MPa the presence of CNT resulted in an increase of $K_\gamma$ from 0.43 to 0.63 and from 0.83 to 0.92, respectively. Similar results were obtained for the same iPP based nanocomposites with 5 wt.% of fibrillated PTFE, which nucleated the crystallization in the γ-form under elevated pressure. The nanocomposites exhibited $K_\gamma$ of about 0.59 and 0.96 at 50 and 100 MPa, respectively [31]. $K_\gamma$ of iPP with nucleating agents crystallized during cooling under 100 MPa did not exceed 0.92 [27,30]. In turn, after nonisothermal crystallization under 50 MPa the high $K_\gamma$ value of 0.85 was reached only in iPP nucleated with 0.4 wt.% of a clarifier 1,3:2,4-bis(3,4-dimethylbenzylidene)sorbitol [30]. This shows that the efficient nucleation of the γ-form increased its content more significantly in the case of cooling under relatively low pressure, at which the γ-domain is relatively narrow. The influence of the nucleants on the γ-content diminished as the γ-domain broadened with increasing crystallization pressure.

Figs. 7a, b and S5 a, b show evolution of DSC heating thermograms of the materials studied crystallized under various pressures. The melting endotherms of neat PP and PP/MT were very similar regardless of the o-MMT content, thus only the thermograms of PP/MT5 are shown. In turn, the thermograms of PP/CN3 and PP/CN5 were also alike, hence only that of PP/CN5 was presented in Figs. 7 and S5. The thermograms show the evolution from melting of the predominant α-form to melting of the pure γ-form. With increasing pressure $T_m$ of PP and PP/MT decreased from 166-168°C to 161°C. The melting endotherms of these materials crystallized under 1.3 MPa were in the form of single peaks. However, with increasing crystallization pressure the low temperature shoulders of these peaks developed and became the most pronounced at 200 and 300 MPa. The thermograms of PP/CN crystallized under 1.3 MPa were similar to those of the other materials crystallized under the same pressure, with single melting peaks with $T_m$ of 167-168°C. At 50 MPa the melting peak of PP/CN1 with $T_m$ of 166°C was featured with low temperature shoulder, which was larger than those observed for PP and PP/MT. At 100 MPa this shoulder developed into low temperature peak with $T_m$ of 158°C. PP/CN3 and PP/CN5 exhibited double-melting behavior already at 50 MPa, with $T_m$ of 160°C and 167°C. During heating of PP/CN1, which crystallized under 200-300 MPa, and two other PP/CN, which crystallized under 100-300 MPa, only single melting peaks were observed, with $T_m$ of 156-155°C and with small high temperature shoulders. The melting temperature of the γ-form is lower than that of the α-form, and, according to the discussion of Mezghani and Phillips [26], during heating at 10 K/min the melting of the γ-form occurs rather than its transformation to the α-form.

The increase of low temperature parts of the melting endotherms of the materials with rising crystallization pressure can be correlated with the increasing γ-content. The higher γ-content also can be the reason of the stronger low temperature melting in PP/CN, especially PP/CN3 and PP/CN5 crystallized under 50-100 MPa, with respect to that of PP and PP/MT crystallized under the same pressure. Thus, the low- and high-temperature parts of the endotherms observed at 50 and 100 MPa can be attributed to the melting of the γ- and α-form, respectively, although the reorganization in the crystalline phase cannot be entirely excluded. It should be noted that the materials crystallized during cooling under 200 and 300 MPa contained solely or almost solely the γ-form. Therefore, it seems that the shoulders of the melting peaks of these materials are related to reorganization in the less stable fraction of γ-phase crystallized in the lower temperature range reached during cooling. As $T_c$s of PP/CN, especially PP/CN3 and PP/CN5, exceeded those of PP and PP/MT, a smaller fraction of γ-crystals recrystallized in PP/CN into more stable phase melting at a higher temperature.

This is well seen in the thermograms of the materials crystallized under 300 MPa containing the pure γ-phase. The melting peaks of PP

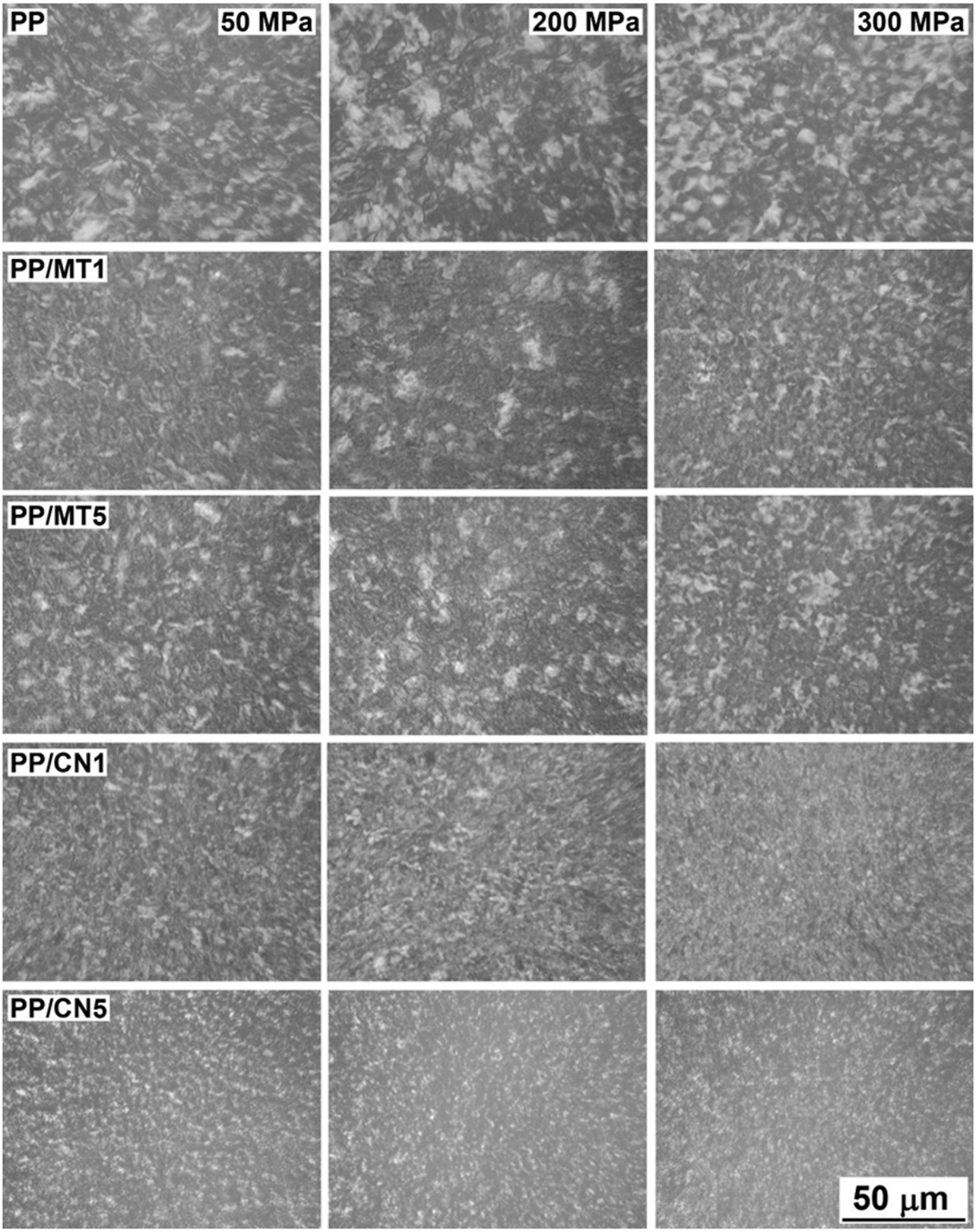


**Fig. 4.** PLM micrographs of thin sections of neat PP and nanocomposites PP/MT1, PP/MT5, PP/CN1, PP/CN5 crystallized during cooling under various pressures.

and PP/MT with $T_m$ of 161°C showed low temperature shoulders located close to 153°C. In turn, the melting peaks of PP/CN1 and PP/CN5 with $T_m$ of 155 -156°C were featured with a large shoulder and a small shoulder, respectively, both near 162°C. The development of the low temperature shoulders in the main peaks with $T_m$ of 155-156°C was accompanied by the reduction of the peaks with $T_m$ of 161°C to the large and then to the small shoulder. This correlates with the increasing $T_c$ of the materials and the decreasing fraction of polymer crystallized in lower temperature range in less stable γ-crystals, susceptible to recrystallization during heating in DSC.

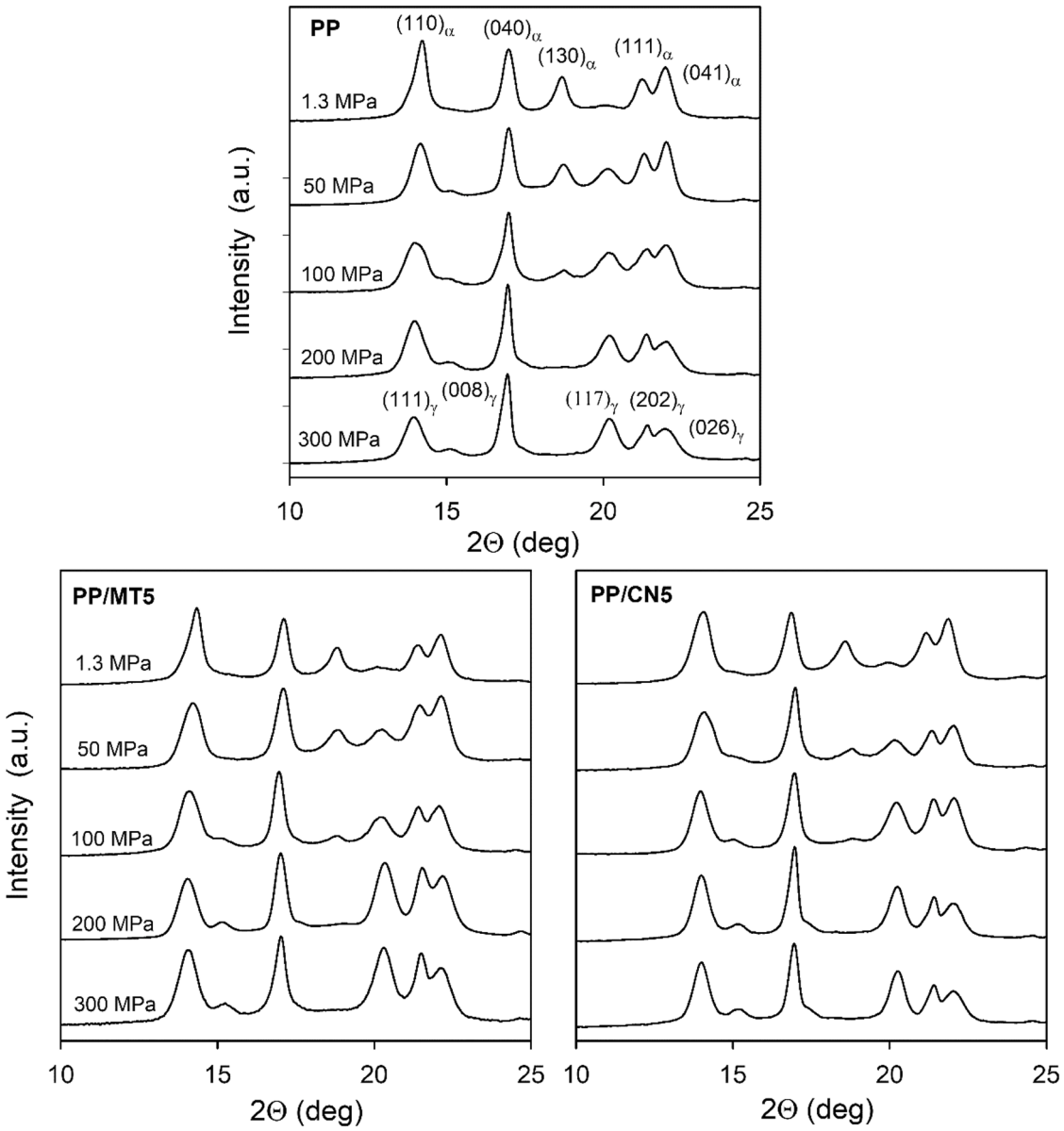


**Fig. 5.** WAXD diffractograms of neat PP, PP/MT5 and PP/CN5 nanocomposites nonisothermally crystallized during cooling under various pressures.

This explanation is supported by DSC thermograms recorded during heating at 30 K/min, which examples are shown in Fig. S6. The thermograms were featured by single peaks with $T_m$s by 1-5 K higher than those measured during slower heating at 10 K/min. The peak shoulders were strongly reduced or absent as the faster heating reduced the reorganization phenomena in the crystalline phase.

Not only $T_m$ depended on the crystallization pressure but also $\Delta H_m$. $\Delta H_m$ of the materials diminished with increasing pressure from 101-105 J/g at 1.3 MPa to 88-91 J/g (calculated per polymer content) at 300 MPa, due to the heat of fusion of the γ-form, 190 J/g, lower than that of the α-form, 209 J/g [26]. Taking into account the predominant α-content in the materials crystallized under 1.3 MPa and the pure γ-phase formed under 300 MPa, the values of $\Delta H_m$ correspond to $X_c$ of the polymer matrix of 48-50% at 1.3 MPa and 46-49% at 300 MPa, confirming that $X_c$ practically did not depend on crystallization pressure. It is worth noting that PP/CN3 and PP/CN5 exhibited the highest $X_c$ values because of the highest $T_c$. Moreover, if the lower values of heat fusion of the α- and γ-crystals are assumed, 167 J/g and 150 J/g [26], the corresponding values of $X_c$, of about 60%, are close to those obtained by WAXD and shown in Fig. 6.

The increase of $T_c$ and the strong reduction of polycrystalline aggregate sizes in PP/CN proved the ability of MWCNT to nucleate the crystallization of iPP in the γ-form under high pressure. Previously [27–31], we demonstrated that nucleants of the iPP α-form under $P_{atm}$ were also efficient in nucleating the high-pressure crystallization of iPP in the γ-form. In view of epitaxy theory, the formation of the heterogeneous α-nuclei of iPP mainly involves the $(010)_\alpha$ plane, and occurs on substrates matching a periodicity of about 0.42, 0.5, or 0.66 nm in this plane. This also applies for the γ-form and involves the equivalent $(001)_\gamma$ plane [76]. However, the epitaxy involving the $(110)_\alpha$ plane with a 0.55-0.56 nm periodicity, is also possible, but it does not apply for the γ-form [77]. It was suggested [28] that the nucleation of iPP crystallization in the γ-form under high pressure could occur directly on the substrates matching periodicity of $(010)_\alpha$ plane (or equivalent $(001)_\gamma$ plane). Another possible mechanism is the nucleation of α-crystals, which serve as nucleation sites for the γ-lamellae, through conventional epitaxy of the γ-crystals on the $(010)_\alpha$ plane [22]. Recently, we have found [29] that the second mechanism prevailed under high pressure in nucleated iPP. According to [26] in the γ-domain the Gibbs free energy of the γ-form crystallization is lower than that of the α-form. However,

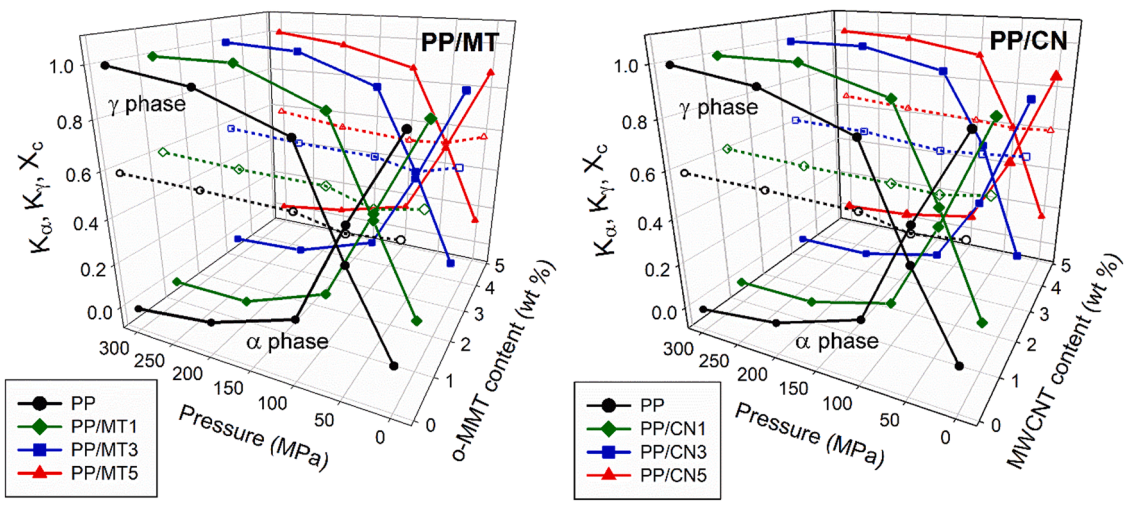


**Fig. 6.** Content of the α- and γ-forms in crystalline phase, $K_\alpha$ and $K_\gamma$ (solid lines, filled symbols), respectively, and crystallinity degree, $X_c$ (dashed lines, empty symbols), of neat PP, PP/MT and PP/CN nanocomposites nonisothermally crystallized during cooling under various pressures.

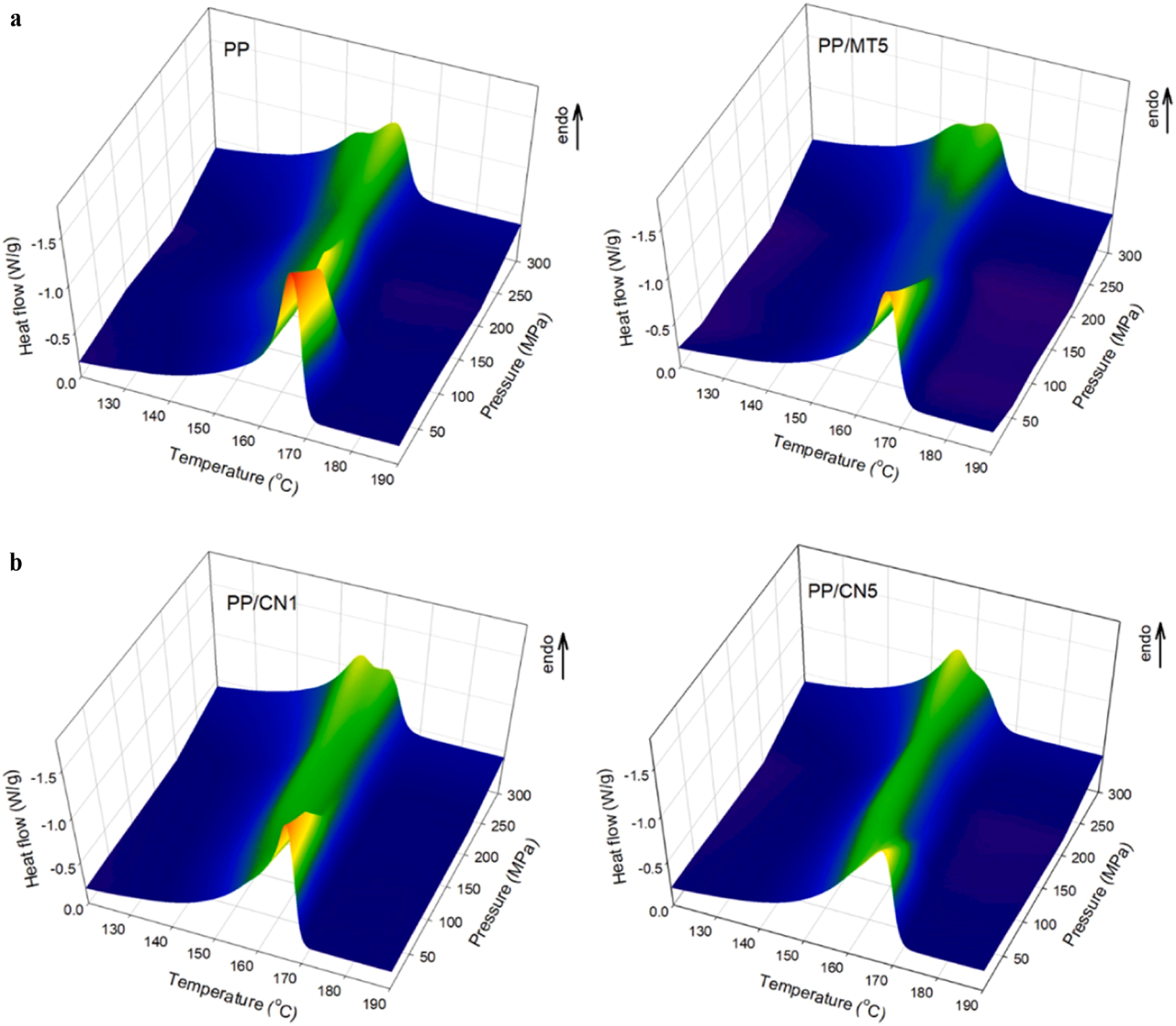


**Fig. 7.** a. Evolution of melting endotherms in DSC heating thermograms of neat PP and PP/MT5 nanocomposite nonisothermlly crystallized during cooling under various pressures, recorded during heating at 10 K/min. b. Evolution of melting endotherms in DSC heating thermograms of PP/CN1 and PP/CN5 nanocomposites nonisothermally crystallized during cooling under various pressures, recorded during heating at 10 K/min.

this does not exclude the formation of a small amount of the α-phase under high pressure, even if not evidenced by WAXD [23,24]. Each several micrometers long α-lamella can serve as a nucleation site for several hundred γ-lamella, as can be estimated based on the lamellae thickness and the long period of γ-iPP crystallized under high pressure [23–25]. The Gibbs free energy barrier for nucleation of the γ-form on the existing α-crystal is strongly decreased compared to that for nucleation on other substrates, even those very efficient. Thus, the direct growth of γ-lamellae from substrates, even if occurs, is much less efficient in the nucleation of crystallization in the γ-phase under high pressure than the nucleation of the α-lamellae, and subsequent growth of the γ-lamellae on them. Most possibly, the latter mechanism also acted during crystallization in the PP/CN under high pressure.

## 4. Conclusion

Nanocomposites of PP with 1-5 wt.% of either o-MMT (PP/MT) or MWCNT (PP/CN) were prepared. Crystallization during cooling under elevated pressure, up to 300 MPa, of the nanocomposites and neat PP was conducted. Temperature of peak crystallization rate ($T_c$) was determined in each case and the structure formed in the materials during the crystallization was examined. Increasing pressure increased $T_c$s of all materials during cooling and the content of the γ-crystallographic form in the crystalline phase. Under 200 and 300 MPa all materials crystallized in nearly pure or pure γ-form. $K_\gamma$ increased from 0.1-0.16 at 1.3 MPa to 1.0 at 300 MPa. PP/MT nanocomposites behaved similarly to neat PP. The $T_c$s and polycrystalline aggregate sizes of PP/MT were similar to those of neat PP.

On the contrary, $T_c$s of PP/CN nanocomposites, especially with 3 and 5 wt. % of MWCNT were markedly higher than those of neat PP in the entire pressure range studied, by 8-13 K, evidencing nucleating activity of the nanofiller. The strong nucleation in PP/CN nanocomposites led to crystallization in the form of fine grains. These results demonstrated the ability of MWCNT to nucleate PP crystallization in the high-pressure γ-form. The crystallization in the higher temperature range from numerous nucleation sites allowed a larger portion of the polymer to solidify in the γ-domain before the temperature reached the α-domain. As a result, the γ-content in PP/CN nanocomposites crystallized under the pressure up to 200 MPa, especially 50-100 MPa, was higher than in PP and PP/MT nanocomposites crystallized under the same pressures. The ability of MWCNT to increase $T_c$ and the γ-content, and simultaneously reduce the grain size in iPP, in the course of nonisothermal crystallization during cooling under high pressure is important during industrial processing like injection molding.

## Funding sources

Grant no. 2018/29/B/ST8/02821 from National Science Centre (Narodowe Centrum Nauki), Poland, and statutory funds of CMMS PAS.

## Notes

Original data may be provided by the corresponding author in justified cases.

## CRediT authorship contribution statement

**Przemyslaw Sowinski:** Conceptualization, Formal analysis, Investigation, Methodology, Supervision, Visualization, Writing – original draft, Writing – review & editing. **Sivanjineyulu Veluri:** Investigation, Visualization, Writing – original draft, Writing – review & editing. **Ewa Piorkowska:** Conceptualization, Formal analysis, Funding acquisition, Methodology, Project administration, Supervision, Writing – original draft, Writing – review & editing. **Konrad Kwiecinski:** Investigation. **Severine A.E. Boyer:** Investigation, Methodology, Writing – review & editing. **Jean-Marc Haudin:** Methodology, Supervision, Writing – review & editing.

## Declaration of Competing Interest

The authors declare that they have no known competing financial interests or personal relationships that could have appeared to influence the work reported in this paper.

## Data availability

Data will be made available on request.

## Acknowledgments

Grant no. 2018/29/B/ST8/02821 from National Science Centre (Narodowe Centrum Nauki), Poland, and statutory funds of CMMS PAS. The authors would like to honor the memory of Bernhard Wunderlich, whom E.P. and J-M.H. had an opportunity to meet, for his outstanding achievements in the field of thermal behavior of polymer materials. His three books on Macromolecular Physics were references for the authors.

## Supplementary materials

Supplementary material associated with this article can be found, in the online version, at doi:10.1016/j.tca.2022.179318.

## References

[1] A.J. Lovinger, J.O. Chua, C.C. Gryte, Studies on the α and β forms of isotactic polypropylene by crystallization in a temperature gradient, J. Polym. Sci. Polym. Phys. Ed. 15 (1977) 641–656, https://doi.org/10.1002/pol.1977.180150405.
[2] A. Mollova, R. Androsch, D. Mileva, M. Gahleitner, S.S. Funari, Crystallization of isotactic polypropylene containing beta-phase nucleating agent at rapid cooling, Eur. Polym. J. 49 (2013) 1057–1065, https://doi.org/10.1016/j.eurpolymj.2013.01.015.
[3] J. Varga, β-modification of isotactic polypropylene: preparation, structure, processing, properties, and application, J. Macromol. Sci. Part B Phys. B41 (2002) 1121–1171, https://doi.org/10.1081/MB-120013089.
[4] D. Mileva, R. Androsch, E. Zhuravlev, C. Shick, B. Wunderlich, Formation and reorganization of the mesophase of isotactic polypropylene, Mol. Cryst. Liq. Cryst. 556 (2012) 74–83, https://doi.org/10.1080/15421406.2012.635912.
[5] B. Lotz, S. Graff, J.C. Wittmann, Crystal morphology of the γ (triclinic) phase of isotactic polypropylene and its relation to the α phase, J. Polym. Sci. Part B Polym. Phys. 24 (1986) 2017–2032, https://doi.org/10.1002/polb.1986.090240909.
[6] D.R. Morrow, B.A. Newman, Crystallization of low-molecular-weight polypropylene fractions, J. Appl. Phys. 39 (1968) 4944–4950, https://doi.org/10.1063/1.1655891.
[7] M. Kojima, Solution-grown lamellar crystals of thermally decomposed isotactic polypropylene, J. Polym. Sci. Part B Polym. Lett. 5 (1967) 245–250, https://doi.org/10.1002/pol.1967.110050307.
[8] A. Turner-Jones, Development of the γ-crystal form in random copolymers of propylene and their analysis by DSC and X-ray methods, Polymer 12 (1971) 487–508, https://doi.org/10.1016/0032-3861(71)90031-0.
[9] G.P. Guidetti, P. Busi, I. Giulianelli, R. Zannetti, Structure-properties relationships in some random co-polymers of propylene, Eur. Polym. J. 19 (1983) 757–759, https://doi.org/10.1016/0014-3057(83)90144-1.
[10] M. Avella, E. Martuscelli, G. Della Volpe, A. Segre, E. Rossi, T. Simonazzi, Composition-properties relationships in propene-ethene random copolymers obtained with high-yield Ziegler-Natta supported catalysts, Makromol. Chem. 187 (1986) 1927–1943, https://doi.org/10.1002/macp.1986.021870812.
[11] A. Marigo, C. Marega, R. Zannetti, G. Paganetto, E. Canossa, F. Coletta, F. Gottardi, Crystallization of the γ-form of isotactic poly(propylene), Makromol. Chem. 190 (1989) 2805–2813, https://doi.org/10.1002/macp.1989.021901112.
[12] D. Fischer, R. Mulhaupt, The influence of regio- and stereoirregularities on the crystallization behavior of isotactic poly(propylene)s prepared with homogeneous group IVa metallocene/methylaluminoxane Ziegler-Natta catalysts, Macromol. Chem. Phys. 195 (1994) 1433–1441, https://doi.org/10.1002/macp.1994.021950426.
[13] C. De Rosa, F. Auriemma, M. Paolillo, L. Resconi, I. Camurati, Crystallization behavior and mechanical properties of regiodefective, highly stereoregular isotactic polypropylene: Effect of regiodefects versus stereodefects and influence of the molecular mass, Macromolecules 38 (2005) 9143–9154, https://doi.org/10.1021/ma051004x.
[14] R. Thomann, H. Semke, R.D. Maier, Y. Thomann, J. Scherble, R. Mulhaupt, J. Kressler, Influence of stereoirregularities on the formation of the γ-phase in

isotactic polypropene, Polymer 42 (2001) 4597–4603, https://doi.org/10.1016/S0032-3861(00)00675-3.
[15] J.L. Kardos, A.W. Christiansen, E. Baer, Structure of pressure-crystallized polypropylene, J. Polym. Sci. Part A2 Polym. Phys. 4 (1966) 777–788, https://doi.org/10.1002/pol.1966.160040509.
[16] K. Mezghani, P.J. Phillips, The γ-phase of high molecular weight isotactic polypropylene. II: The morphology of the γ-form crystallized at 200 MPa, Polymer 38 (1997) 5725–5733, https://doi.org/10.1016/S0032-3861(97)00131-6.
[17] B. Lotz, J. Ruan, A. Thierry, G.C. Alfonso, A. Hiltner, E. Baer, E. Piorkowska, A. Galeski, A Structure of copolymers of propene and hexene isomorphous to isotactic poly(1-butene) form I, Macromolecules 39 (2006) 5777–5781, https://doi.org/10.1021/ma052314i.
[18] C. De Rosa, F. Auriemma, P. Corradini, O. Tarallo, S. Dello Iacono, E. Ciaccia, L. Resconi, Crystal structure of the trigonal form of isotactic polypropylene as an example of density-driven polymer structure, J. Am. Chem. Soc. 128 (2006) 80–81, https://doi.org/10.1021/ja0572957.
[19] B. Lotz, A new ε crystal modification found in stereodefective isotactic polypropylene samples, Macromolecules 47 (2014) 7612–7624, https://doi.org/10.1021/ma5009868.
[20] S.V. Meiile, S. Bruckner, Non-parallel chains in crystalline γ-isotactic polypropylene, Nature 340 (1989) 455–457, https://doi.org/10.1038/340455a0.
[21] S.V. Meille, S. Bruckner, W. Porzio, γ-Isotactic polypropylene. A structure with nonparallel chain axes, Macromolecules 23 (1990) 4114–4121, https://doi.org/10.1021/ma00220a014.
[22] B. Lotz, S. Graff, C. Straupe, J.C. Wittmann, Single crystals of γ phase isotactic polypropylene: combined diffraction and morphological support for a structure with non-parallel chains, Polymer 32 (1991) 2902–2910, https://doi.org/10.1016/0032-3861(91)90185-L.
[23] E. Lezak, Z. Bartczak, A. Galeski, Plastic deformation of the γ phase in isotactic polypropylene in plane-strain compression, Macromolecules 39 (2006) 4811–4819, https://doi.org/10.1021/ma0605907.
[24] C. von Baeckmann, H. Wilhelm, F. Spieckermann, S. Strobel, G. Polt, P. Sowinski, E. Piorkowska, A. Bismarck, M Zehetbauer, The influence of crystallization conditions on the macromolecular structure and strength of γ-polypropylene, Thermochim. Acta 677 (2019) 131–138, https://doi.org/10.1016/j.tca.2019.03.007.
[25] M. Slouf, E. Pavlova, S. Krejcikova, A. Ostafinska, A. Zhigunov, V. Krzyzanek, P. Sowinski, E. Piorkowska, Relations between morphology and micromechanical properties of alpha, beta and gamma phases of iPP, Polym. Test. 67 (2018) 522–532, https://doi.org/10.1016/j.polymertesting.2018.03.039.
[26] K. Mezghani, P.J. Phillips, The γ-phase of high molecular weight isotactic polypropylene: III. The equilibrium melting point and the phase diagram, Polymer 39 (1998) 3735–3744, https://doi.org/10.1016/S0032-3861(97)10121-5.
[27] P. Sowinski, E. Piorkowska, S.A.E. Boyer, J.M. Haudin, Nucleation of crystallization of isotactic polypropylene in the gamma form under high pressure in nonisothermal conditions, Eur. Polym. J. 85 (2016) 564–574, https://doi.org/10.1016/j.eurpolymj.2016.10.055.
[28] P. Sowinski, E. Piorkowska, S.A.E. Boyer, J.M. Haudin, K. Zapala, The role of nucleating agents in high-pressure-induced gamma crystallization in isotactic polypropylene, Colloid Polym. Sci. 293 (2015) 665–675, https://doi.org/10.1007/s00396-014-3445-z.
[29] P. Sowinski, E. Piorkowska, S.A.E. Boyer, J.M. Haudin, On the structure and nucleation mechanism in nucleated isotactic polypropylene crystallized under high pressure, Polymer 151 (2018) 179–186, https://doi.org/10.1016/j.polymer.2018.07.056.
[30] P. Sowinski, E. Piorkowska, S.A.E. Boyer, J.M. Haudin, High-pressure crystallization of iPP nucleated with 1,3:2,4-bis(3,4-dimethylbenzylidene)sorbitol, Polymers 13 (2021) 145, https://doi.org/10.3390/polym13010145.
[31] P. Sowinski, S. Veluri, E. Piorkowska, Crystallization of isotactic polypropylene nanocomposites with fibrillated poly(tetrafluoroethylene) under elevated pressure, Polymers 14 (2022) 88, https://doi.org/10.3390/polym14010088.
[32] S. Galeski, E. Piorkowska, A. Rozanski, G. Regnier, A. Galeski, K. Jurczuk, Crystallization kinetics of polymer fibrous nanocomposites, Eur. Polym. J. 83 (2016) 181–201, https://doi.org/10.1016/j.eurpolymj.2016.08.002.
[33] Y. Qiao, A. Jalali, J. Yang, Y. Chen, S. Wang, Y. Jiang, J. Hou, J. Jiang, Q. Li, C. B. Park, Non-isothermal crystallization kinetics of polypropylene/polytetrafluoroethylene fibrillated composites, J. Mater. Sci. 56 (2021) 3562–3575, https://doi.org/10.1007/s10853-020-05328-5.
[34] G.G. Kaya, H. Deveci, Synergistic effects of silica aerogels/xerogels on properties of polymer composites: a review, J. Ind. Eng. Chem. 89 (2020) 13–27, https://doi.org/10.1016/j.jiec.2020.05.019.
[35] M.J. Mochane, J.S. Sefadi, T.S. Motsoeneng, T.E. Mokoena, T.G. Mofokeng, T. C. Mokhena, The effect of filler localization on the properties of biopolymer blends, recent advances: a review, Polym. Compos. 41 (2020) 2958–2979, https://doi.org/10.1002/pc.25590.
[36] M. Moniruzzaman, K.I. Winey, Polymer nanocomposites containing carbon nanotubes, Macromolecules 39 (2006) 5194–5205, https://doi.org/10.1021/ma060733p.
[37] B.V. Basheer, J.J. George, S. Siengchin, J. Parameswaranpillai, Polymer grafted carbon nanotubes—synthesis, properties, and applications: a review, Nano Struct. Nano Objects 22 (2020), 100429, https://doi.org/10.1016/j.nanoso.2020.100429.
[38] K. Chrissafis, D. Bikiaris, Can nanoparticles really enhance thermal stability of polymers? Part I: an overview on thermal decomposition of addition polymers, Thermochim. Acta 523 (2011) 1–24, https://doi.org/10.1016/j.tca.2011.06.010.
[39] V. Sivanjineyulu, K. Behera, Y.H. Chang, F.C. Chiu, Selective localization of carbon nanotube and organoclay in biodegradable poly(butylene succinate)/polylactide blend-based nanocomposites with enhanced rigidity, toughness and electrical conductivity, Compos. Part A Appl. Sci. Manuf. 114 (2018) 30–39, https://doi.org/10.1016/j.compositesa.2018.08.009.
[40] V. Sivanjineyulu, Y.H. Chang, F.C. Chiu, Characterization of carbon nanotube- and organoclay-filled polypropylene/poly(butylene succinate) blend-based nanocomposites with enhanced rigidity and electrical conductivity, J. Polym. Res. 24 (2017) 130, https://doi.org/10.1007/s10965-017-1289-1.
[41] B.S. Bouakaz, A. Habi, Y. Grohens, I. Pillin, Organomontmorillonite/graphene-PLA/PCL nanofilled blends: new strategy to enhance the functional properties of PLA/PCL blend, Appl. Clay. Sci. 139 (2017) 81–91, https://doi.org/10.1016/j.clay.2017.01.014.
[42] D. Bikiaris, Microstructure and properties of polypropylene/carbon nanotube nanocomposites, Materials 3 (2010) 2884–2946, https://doi.org/10.3390/ma3042884.
[43] E. Manias, A. Touny, L. Wu, K. Strawhecker, B. Lu, T.C. Chung, Polypropylene/montmorillonite nanocomposites. Review of the synthetic routes and materials properties, Chem. Mater. 13 (2001) 3516–3523, https://doi.org/10.1021/cm0110627.
[44] S.S. Ray, M. Okamoto, Polymer/layered silicate nanocomposites: a review from preparation to processing, Prog. Polym. Sci. 28 (2003) 1539–1641, https://doi.org/10.1016/j.progpolymsci.2003.08.002.
[45] H. Deng, T. Skipa, R. Zhang, D. Lellinger, E. Bilotti, I. Alig, T. Peijs, Effect of melting and crystallization on the conductive network in conductive polymer composites, Polymer 50 (2009) 3747–3754, https://doi.org/10.1016/j.polymer.2009.05.016.
[46] M.K. Seo, S.J. Park, Electrical resistivity and rheological behaviors of carbon nanotubes-filled polypropylene composites, Chem. Phys. Lett. 395 (2004) 44–48, https://doi.org/10.1016/j.cplett.2004.07.047.
[47] E. Piorkowska, Crystallization in polymer composites and nanocomposites, in: E. Piorkowska, G.C. Rutledge (Eds.), Handbook of Polymer Crystallization, Wiley, Hoboken, 2013, pp. 379–398, https://doi.org/10.1002/9781118541838.
[48] D. Xu, Z. Wang, Role of multi-wall carbon nanotube network in composites to crystallization of isotactic polypropylene matrix, Polymer 49 (2008) 330–338, https://doi.org/10.1016/j.polymer.2007.11.041.
[49] E. Assouline, A. Lustiger, A.H. Barber, C.A. Cooper, E. Klein, E. Wachtel, H. D. Wagner, Nucleation ability of multiwall carbon nanotubes in polypropylene composites, J. Polym. Sci. Part B Polym. Phys. 41 (2003) 520–527, https://doi.org/10.1002/polb.10394.
[50] W. Leelapornpisit, M.T. Ton-That, F. Perrin-Sarazin, K.C. Cole, J. Denault, B. Simard, Effect of carbon nanotubes on the crystallization and properties of polypropylene, J. Polym. Sci. Part B Polym. Phys. 43 (2005) 2445–2453, https://doi.org/10.1002/polb.20527.
[51] L. Valentini, J. Biagiotti, J.M. Kenny, S. Santucci, Morphological characterization of single-walled carbon nanotubes-PP composites, Compos. Sci. Technol. 63 (2003) 1149–1153, https://doi.org/10.1016/S0266-3538(03)00036-8.
[52] Y. Peneva, M. Valcheva, L. Minkova, M. Micusik, M. Omastova, Nonisothermal crystallization kinetics and microhardness of PP/CNT composites, J. Macromol. Sci. Part B Phys. 47 (2008) 1197–1210, https://doi.org/10.1080/00222340802403420.
[53] K.B. Lu, N. Grossiord, C.E. Koning, H.E. Miltner, B. van Mele, J. Loos, Carbon nanotube/isotactic polypropylene composites prepared by latex technology: morphology analysis of CNT-induced nucleation, Macromolecules 41 (2008) 8081–8085, https://doi.org/10.1021/ma8008299.
[54] B.P. Grady, F. Pompeo, R.L. Shambaugh, D.E. Resasco, Nucleation of polypropylene crystallization by single-walled carbon nanotubes, J. Phys. Chem. B 106 (2002) 5852–5858, https://doi.org/10.1021/jp014622y.
[55] S. Zhang, M.L. Minus, L.B. Zhu, C.P. Wong, S. Kumar, Polymer transcrystallinity induced by carbon nanotubes, Polymer 49 (2008) 1356–1364, https://doi.org/10.1016/j.polymer.2008.01.018.
[56] J.M. Lin, S.G. Yang, B.C. Hu, Y.N. Song, J.Y. Ren, J. Lei, X. Ji, Z.M. Li, Quantification of pressure-induced γ-crystals in isotactic polypropylene: The influence of shear and carbon nanotubes, Polym. Cryst. 1 (2018) e10002, https://doi.org/10.1002/pcr2.10002.
[57] K. Wang, C. Tang, P. Zhao, H. Yang, Q. Zhang, R. Du, Q. Fu, Rheological investigations in understanding shear-enhanced crystallization of isotactic poly(propylene)/multi-walled carbon nanotube composites, Macromol. Rapid Commun. 28 (2007) 1257–1264, https://doi.org/10.1002/marc.200700069.
[58] S. Hambir, N. Bulakh, J.P. Jog, Polypropylene/Clay nanocomposites: effect of compatibilizer on the thermal, crystallization and dynamic mechanical behavior, Polym. Eng. Sci. 42 (2002) 1800–1807, https://doi.org/10.1002/pen.11072.
[59] P. Maiti, P.H. Nam, M. Okamoto, N. Hasegawa, A. Usuki, Influence of crystallization on intercalation, morphology, and mechanical properties of polypropylene/clay nanocomposites, *Macromolecule*s 35 (2002) 2042–2049, https://doi.org/10.1021/ma010852z.
[60] W. Xu, M. Ge, P. He, Nonisothermal crystallization kinetics of polypropylene/montmorillonite nanocomposites, J. Polym. Sci. Part B Polym. Phys. 40 (2002) 408–414, https://doi.org/10.1002/polb.10101.
[61] A. Pozsgay, T. Fráter, L. Papp, I. Sajó, B. Pukánszky, Nucleating effect of montmorillonite nanoparticles in polypropylene, J. Macromol. Sci. Part B Phys. 41 (2002) 1249–1265, https://doi.org/10.1081/MB-120013095.
[62] P. Maiti, P.H. Nam, M. Okamoto, T. Kotaka, N. Hasegawa, A. Usuki, The effect of crystallization on the structure and morphology of polypropylene/clay nanocomposites, Polym. Eng. Sci. 42 (2002) 1864–1871, https://doi.org/10.1002/pen.11079.

[63] F. Perrin-Sarazin, M.T. Ton-That, M.N. Bureau, J. Denault, Micro- and nano-structure in polypropylene/clay nanocomposites, Polymer 46 (2005) 11624–11634, https://doi.org/10.1016/j.polymer.2005.09.076.
[64] P. Svoboda, C. Zeng, H. Wang, L.J. Lee, D.L. Tomasko, Morphology and mechanical properties of polypropylene/organoclay nanocomposites, J. Appl. Polym. Sci. 85 (2002) 1562–1570, https://doi.org/10.1002/app.10789.
[65] Q. Yuan, V.G. Rajan, R.D.K. Misra, Nanoparticle effects during pressure-induced crystallization of polypropylene, Mater. Sci. Eng. Part B 153 (2008) 88–95, https://doi.org/10.1016/j.mseb.2008.10.031.
[66] R.D.K. Misra, Q. Yuan, J. Chen, Y. Yang, Hierarchical structures and phase nucleation and growth during pressure-induced crystallization of polypropylene containing dispersion of nanoclay: the impact on physical and mechanical properties, Mater. Sci. Eng. A 527 (2010) 2163–2181, https://doi.org/10.1016/j.msea.2009.11.023.
[67] E. Szkudlarek, E. Piorkowska, S.A.E. Boyer, J.M. Haudin, K. Gadzinowska, Nonisothermal shear-induced crystallization of polypropylene-based composite materials with montmorillonite, Eur. Polym. J. 49 (2013) 2109–2119, https://doi.org/10.1016/j.eurpolymj.2013.04.029.
[68] A. Rozanski, B. Monasse, E. Szkudlarek, A. Pawlak, E. Piorkowska, A. Galeski, J. M. Haudin, Shear-induced crystallization of isotactic polypropylene based nanocomposites with montmorillonite, Eur. Polym. J. 45 (2009) 88–101, https://doi.org/10.1016/j.eurpolymj.2008.10.011.
[69] BYK Cloisite 15A Nanoclay, https://www.lookpolymers.com/pdf/BYK-Cloisite-15A-Nanoclay.pdf, accessed on August 11, 2022.
[70] Technical data sheet: NC7000 (2016), https://www.nanocyl.com/wp-content/uploads/2016/07/DM-TI-02-TDS-NC7000-V08.pdf, accessed on August 11, 2022.
[71] T. Kazmierczak, A. Galeski, Transformation of polyethylene crystals by high-pressure annealing, J. Appl. Polym. Sci. 86 (2002) 1337–1350, https://doi.org/10.1002/app.11275.
[72] M. Rabiej, Application of immune and genetic algorithms to the identification of a polymer based on its X-ray diffraction curve, J. Appl. Crystallogr. 46 (2013) 1136–1144, https://doi.org/10.1107/S0021889813015987.
[73] A.Turner Jones, J.M. Aizlewood, D.R. Beckett, Crystalline forms of isotactic polypropylene, Makrom. Chem. 75 (1964) 134–158, https://doi.org/10.1002/macp.1964.020750113.
[74] A. Leszczyńska, J. Njuguna, K. Pielichowski, J.R Banerjee, Polymer/montmorillonite nanocomposites with improved thermal properties: part I. Factors influencing thermal stability and mechanisms of thermal stability improvement, Thermochim. Acta 453 (2007) 75–96, https://doi.org/10.1016/j.tca.2006.11.002.
[75] C. Angelloz, R. Fulchiron, A. Douillard, B. Chabert, R. Fillit, A. Vautrin, L. David, Crystallization of isotactic polypropylene under high pressure (γ phase), Macromolecules 33 (2000) 4138–4145, https://doi.org/10.1021/ma991813e.
[76] C. Mathieu, A. Thierry, J.C. Wittmann, B. Lotz, "Multiple" nucleation of the (010) contact face of isotactic polypropylene, α phase, Polymer 41 (2000) 7241–7253, https://doi.org/10.1016/S0032-3861(00)00062-8.
[77] S. Yan, F. Katzenberg, J. Petermann, D. Yang, Y. Shen, C. Straupe, J.C. Wittmann, B. Lotz, A novel epitaxy of isotactic polypropylene (α phase) on PTFE and organic substrates, Polymer 41 (2000) 2613–2625, https://doi.org/10.1016/S0032-3861(99)00310-9.